

# A calorimetric study of the temperature effect on Calcium Phosphate precipitation

Anastasios I. Mitsionis · Tiverios C. Vaimakis

MEDICTA2009 Conference  
© Akadémiai Kiadó, Budapest, Hungary 2009

**Abstract** The precipitation of calcium phosphate was studied using a heat flow twin calorimeter (C80, Setaram, France). The process was carried out using two identical membrane vessels. In the lower parts of both vessels 2 mL of a supersaturated solution (solution A) containing  $\text{Ca}(\text{H}_2\text{PO}_4)\cdot 2\text{H}_2\text{O}$  (0.054 M) and  $\text{CaCl}_2\cdot\text{H}_2\text{O}$  (0.125 M) with a molar ratio  $\text{Ca}/\text{P} = 1.67$  were added. Then 0.05 mL of an ammonium solution (25% w/w) (solution B) and 0.05 mL of distilled water were transferred in the upper parts of sample and reference vessels, respectively. After temperature had been maintained at 303, 313, 323 and 333 K the membranes of both sample and reference vessels were broken simultaneously. The precipitation process also repeated with the same conditions for periods of 15, 60 and 120 min in a bath. The first two calorimetric curves (303, 313 K) show a single exothermic step during the process as a sharp peak in the initial stage. On the contrary at the experimental temperature of 323 K except of the sharp peak in the initial stage, a steadily exothermic tendency appears after 100 min time. In higher temperature (333 K) the sharp peak appears in the initial stage followed by a broad exothermic step between 75 and 320 min time. The XRD analyses show that the solids in the initial experimental stages are mainly consisted of dicalcium phosphate dihydrate (DCPD) for the lower temperature and a biphasic or triphasic system consisted of hydroxyapatite (HA), dicalcium phosphate anhydrous (DCPA) and octacalcium phosphate (OCP) for the rest temperatures. The XRD analyses show also that during the solution aging the initial

products are transformed into the more stable thermal forms of HA and octacalcium phosphate (OCP).

**Keywords** Calcium phosphate · Calorimeter · Hydroxyapatite

## Introduction

Calcium phosphates (CaP) are an important category of chemical compounds not only for their excellent biocompatibility, bioactivity and osteoconductivity [1] but also for their thermodynamical stability. Each calcium phosphate compound can lead to new families of phosphate materials of great importance in chemical and natural sciences, depending on its own thermodynamical properties. These properties can be attributed to their morphological and chemical structure of each compound.

So far, a variety of calcium phosphate particles in forms of needle-like nanocrystals [2], nanorods [3], whiskers [4], microtubes [5] and yet spherical particles [6] have obtained in order to achieve the best results for desirable application. The most remarkable CaP material is hydroxyapatite ( $\text{Ca}_{10}(\text{PO}_4)_6(\text{OH})_2$ ; HA). HA exhibits excellent biocompatibility and bioactivity, possibly due to its compositional similarity to hard tissue mineral [7, 8]. Besides its extensively studied application in the reconstruction of damaged tissue [9, 10], its ability to absorb substances of biological interest, makes HA an attractive material for drug delivery systems. Although stoichiometric HA is the less soluble and more stable CaP material, its calcium deficient non-stoichiometric form is the most often synthesized one.

The most common co-precipitated CaP materials are  $\beta$ -tricalcium phosphate ( $\text{Ca}_3(\text{PO}_4)_2$ ;  $\beta$ -TCP), octacalcium phosphate ( $\text{Ca}_8\text{H}_2(\text{PO}_4)_6\cdot 5\text{H}_2\text{O}$ ; OCP), dicalcium phosphate

A. I. Mitsionis · T. C. Vaimakis (✉)  
Department of Chemistry, University of Ioannina,  
P.O. Box 1186, 45110 Ioannina, Greece  
e-mail: tvaimak@cc.uoi.gr

anhydrous ( $\text{CaHPO}_4$ ; DCPA) and dicalcium phosphate dihydrate ( $\text{CaHPO}_4 \cdot 2\text{H}_2\text{O}$ ; DCPD). There are many preparation methods for calcium phosphate materials and the hydrothermal method is the most commonly used due to its simplicity and quickness. Hydrothermal synthesis has been used to transform slurries, solutions, or gels into the desired crystalline phase under mild reaction conditions typically below 700 K [11]. Different factors such as Ca/P molar ratio, trace elements, and sintering temperature affect the density, the chemical composition and then the dissolution and the precipitation processes of HA [12]. According to Bianco et al. synthesis temperature affects the crystallite size, shape factor and crystallinity degree [13]. At this point it is a matter of great importance to determine the way of how, both temperature and reaction time can influence the morphology and the stoichiometry of calcium phosphates.

In our work, we follow the modified precipitation method [14, 15]. According to this method HA is prepared by a rapid increase in the pH value of a solution containing calcium and phosphate ions with molar ratio similar to HA. Afterwards the powders prepared were studied using X-ray diffractometry (XRD), thermogravimetry/differential thermal analysis/differential thermogravimetry (TG/DSC/DTG), Fourier-transform infrared spectroscopy (FT-IR) and  $\text{N}_2$  adsorption-desorption porosimetry.

## Materials and methods

The reagents that have been used were  $\text{CaCl}_2 \cdot 2\text{H}_2\text{O}$  (Fluka, Assay (KT) 99%),  $\text{Ca}(\text{H}_2\text{PO}_4)_2 \cdot \text{H}_2\text{O}$  (Riedel-de Haën, Assay 88%), Citric Acid (Riedel-de Haën, Assay 99.5%) and Ammonia solution 25% (Riedel-de Haën).

The precipitation process was carried out in a heat flow twin calorimeter (Type C.80.II, Setaram, France) using two identical membrane vessels, for the precipitation solution, and for the reference. 2 mL of a supersaturated solution (solution A) containing  $\text{Ca}(\text{H}_2\text{PO}_4)_2 \cdot \text{H}_2\text{O}$  (0.054 M) and  $\text{CaCl}_2 \cdot 2\text{H}_2\text{O}$  (0.125 M) with a molar ratio  $\text{Ca/P} = 1.67$  were put into the lower compartment of each vessel and closed by a thin circular membrane of parafilm. A volume of 0.05 mL of  $\text{NH}_4\text{OH}$  (25% w/w) and 0.05 mL of distilled water were added into the upper compartment of the sample and reference vessels, respectively. The experimental temperature was adjusted at 303, 313, 323 and 333 K. After the complete stabilization of baseline, the membranes of both sample and reference vessels were broken simultaneously by movable rods.

The experiments were run using Setaram software for 330 min and a plot of heat-flow versus time was obtained. The process enthalpy was calculated by peak area integration using the SETSOFT package. The precipitation process was also repeated with the same conditions in

batch experiments for periods of 15, 60 and 120 min in a bath at 303, 313, 323 and 333 K. The solids that have been collected were filtrated, dried for 24 h and then characterized by the above mentioned methods. The samples named according to experiment temperature and aging time in minutes, i.e., sample name 30c60m refers to a material precipitated in 303 K temperature after 60 min aging time.

The identification of the crystal phases in the obtained products was carried out by the X-ray diffraction (XRD) technique, using a Brüker P8 Advance apparatus, with a  $2\theta$  range of  $20^\circ$ – $60^\circ$  in steps of  $0.02^\circ$  and the identification of the patterns was made by the cards of the International Centre for Diffraction Data (ICDD). FT-IR performed using a spectrophotometer (Model Spectrum RX I FT-IR, Perkin-Elmer). The KBr disk technique was used with  $\sim 2$  mg of powder in  $\sim 200$  mg of spectroscopic-grade KBr (Merck), which had been dried at 373 K. Infrared spectra were recorded in the  $4,000$ – $400$   $\text{cm}^{-1}$  region.

The textural properties of the solids were examined by  $\text{N}_2$  adsorption-desorption porosimetry which provides also the pore size distribution, using a Fisons Instruments Sorptomatic 1900. Before  $\text{N}_2$  adsorption-desorption measurement the sample was degassed at 450 K and pressure of 10–30 Torr for 6 h.

Simultaneously TG/DSC (thermogravimetry/differential scanning calorimetry) measurements were carried out by a STA 449C (Netzch-Gerätebau, GmbH, Germany) equipment. The heating range was from room temperature up to 1,300 K, with a heating rate of  $10$   $\text{K min}^{-1}$  under synthetic air flow rate of  $30$   $\text{cm}^3/\text{min}$ .  $\text{Al}_2\text{O}_3$  powder as reference were used.

## Results and discussion

The curves of heat-flow versus time are shown in Fig. 1 and the treatment of the curves in Table 1. After mixing of Solution A with the ammonia solution (time 0 min) a sharp

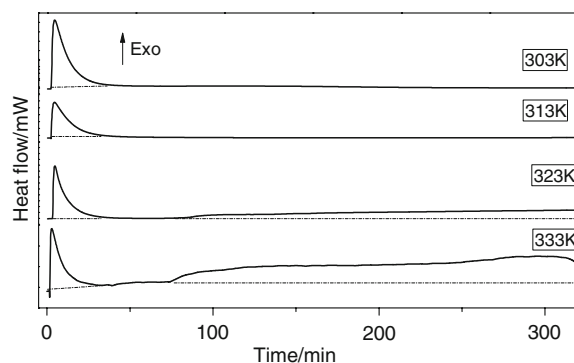


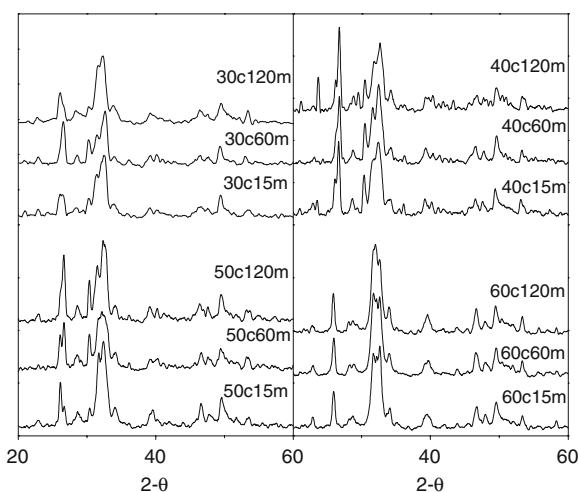
**Fig. 1** Calorimetric curves for samples prepared at 303, 313, 323 and 333 K

**Table 1** Heat flow results summary

Experiment temperature/K	1st stage		2nd stage
	Enthalpy/ J g <sup>-1</sup>	Time yield/min	Enthalpy/ J g <sup>-1</sup>
303	-395.6	41.3	-
313	-359.9	42.9	-
323	-160.8	45.2	-124.7
333	-143.5	48.2	-1217.1

exothermic peak is observed in all experiments. This peak is attributed mainly to the neutralization-precipitation process. The calculated enthalpies as well as the process' time yield of this step are showed in Table 1. As we can see the process enthalpy decreases as the experimental temperature increases. In the following step experiments that took place at temperatures of 303 and 313 K didn't show any change in their curves as time increased, indicating either that no transformations take place after the solution neutralization-precipitation or that transformations occur very slowly. On the contrary the process at 323 K showed a small exothermic tendency between 60 and 330 min time, indicating that transformations take place after the initial precipitation. At temperature of 333 K the heat flow curve shows a weak broad peak between 60 and 330 min time. These observations led us on the repeating the process with the above mentioned hydrothermal method for 15, 60 and 120 min time.

The XRD patterns of the precipitants are depicted in Fig. 2. In general the precipitated materials showed low crystallinity and multiple phases. The analyses showed that in lower temperatures (303, 313 K) the appeared phases were HA, OCP, DCPA and DCPD. The increase of precipitation temperature results to the disappearance of the

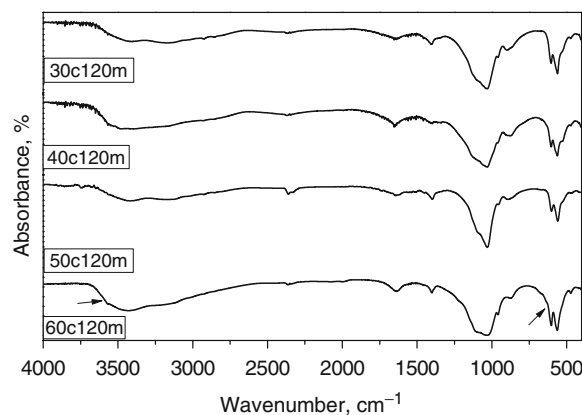
**Fig. 2** XRD Patterns of the precipitated materials

initial DCPD phase and consequently the disappearance of DCPA phase at 323 and 333 K, respectively. These facts indicate that, in higher temperatures, aging time seems to increase the more thermodynamical stable phase, HA. The XRD analysis summary is depicted on Table 2. In general time affects the samples containing both DCPA and DCPD, in a matter of DCPA increase in every sample instead of DCPD.

Figure 3 shows the infrared absorption spectra of the obtained materials precipitated after 120 min aging time. The collected precipitants in the earlier stages (15, 60 min aging time) didn't show any remarkable difference among the temperature scale. In the highest temperature the collected precipitant (60c120m) showed the characteristic absorption bands at 3,570 and 635 cm<sup>-1</sup> that correspond, respectively, to the stretching vibration of the lattice OH<sup>-</sup> ions, indicating the formation of HA phase. The rest of the adsorption bands are depicted in every sample. The broad band at 3,500–3,100 cm<sup>-1</sup> corresponds to adsorbed hydrate. The characteristic bands for PO<sub>4</sub><sup>3-</sup> appear at 963, 610, 560 and 480 cm<sup>-1</sup>. The weak shoulder at 1,260 cm<sup>-1</sup> and a weak peak at 870 cm<sup>-1</sup> can be assigned to P–O–H deformation modes which indicate the presence of the HPO<sub>4</sub><sup>2-</sup> ionic group of both DCPD and DCPA as well as calcium deficient HA.

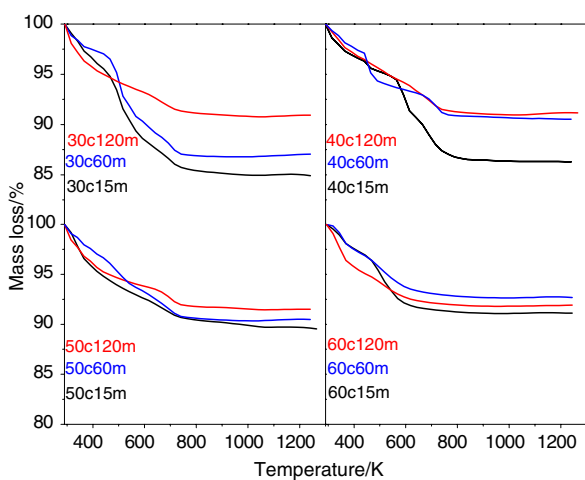
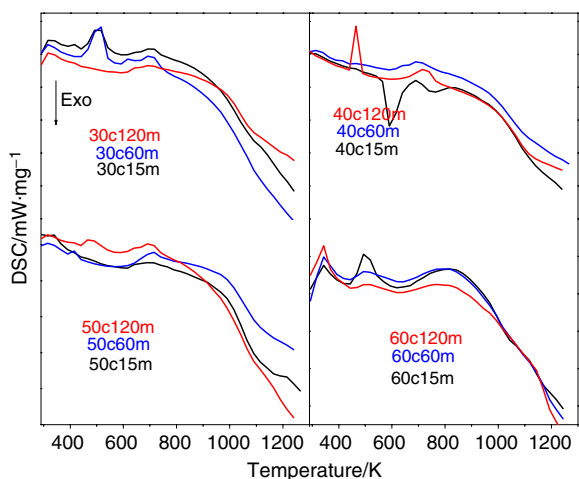
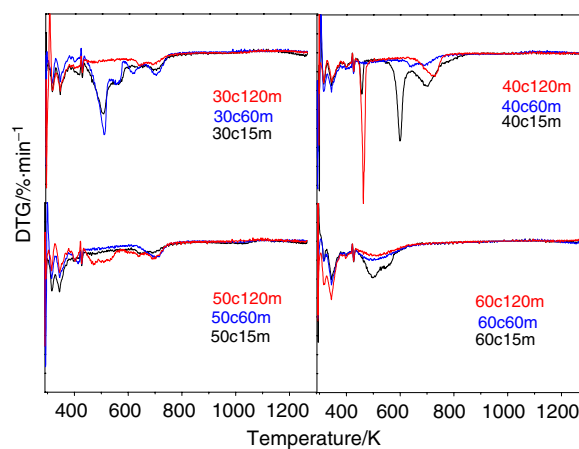
The samples' N<sub>2</sub> adsorption isotherms have the same shape, which is attributed to type III characteristic for non-porous solids. The specific surface area (ssa) for each sample is shown in Table 2. The raise of samples' ssa at 323 K and especially at 333 K can be attributed to the transformation of nonporous materials such as DCPA and DCPD to the more porous materials of HA and OCP which are well known materials for their mesopores appearance due to the inter-spaces between the particles in the aggregates.

Figures 4 and 5 show the TG and DSC curves of the precipitated materials, respectively. The thermal transformations of samples take place in five not distinguished

**Fig. 3** FT-IR spectra of samples prepared after 120 min aging time. Arrows denote OH<sup>-</sup> stretching vibrations

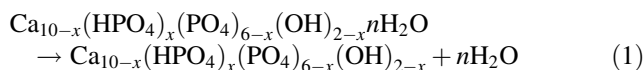
**Table 2** XRD, N<sub>2</sub> porosimetry and TG/DSC results summary

Sample name	Crystal phases	SSa/m <sup>3</sup> g <sup>-1</sup>	Mass loss (%) partial				
			293–373 K	373–700 K	700–850 K	850–1,050 K	1,050–1,300 K
30c15m	HA, OCP, DCPA, DCPD	44.4	2.82	8.77	3.13	0.32	0.71
30c60m	>>	33.8	2.67	7.60	3.25	0.06	0.16
30c120m	>>	49.5	3.76	3.15	2.04	0.25	0.41
40c15m	>>	44.7	2.69	5.37	5.45	0.21	0.20
40c60m	>>	40.4	2.52	3.51	2.86	0.15	0.37
40c120m	>>	48.7	1.98	4.69	2.55	0.12	0.35
50c15m	HA, OCP, DCPA	58.3	3.64	3.89	2.16	0.33	0.77
50c60m	>>	64.5	3.34	2.88	2.04	0.14	0.39
50c120m	>>	40.1	3.17	3.72	2.60	0.14	0.37
60c15m	HA, OCP	88.8	4.01	4.00	0.82	0.08	0.18
60c60m	>>	82.3	2.08	4.29	0.91	0.07	0.17
60c120m	>>	94.5	3.79	3.60	0.76	0.05	0.19

**Fig. 4** TG curves of precipitated samples**Fig. 5** DSC curves of precipitated samples**Fig. 6** DTG curves of precipitated samples

steps. The DTG curves (Fig. 6) help us to distinguish the stages that take place in this process. Using the NETZSCH SEPARATION OF PEAKS software (SW/ PKS/ 650.01A) from ambient temperature to 1,300 K we calculated the partial mass loss of each step as is depicted in Table 2.

The first step, which is consisted of 2 stages with a total mass loss of ~3.0%, shows an endothermic peak between room temperature and ~373 K and it can be attributed to the removal of absorbed water as well as other adsorbed volatile compounds (reaction 1).



The second step (~373–700 K), is consisted of three stages with total mass loss ~5.0%, can attributed mainly to the removal of crystalline water by DCPD and OCP. In this step the transformation of DCPD to DCPA (reaction 2) and the OCP dehydration (reaction 3) takes place.

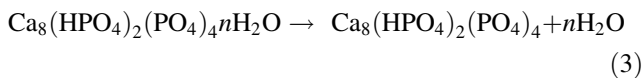
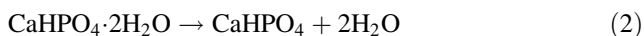
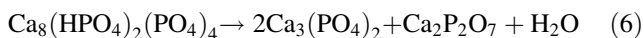
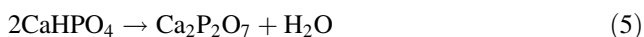
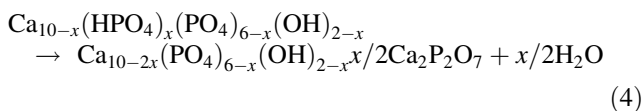
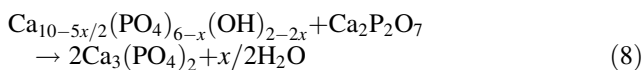
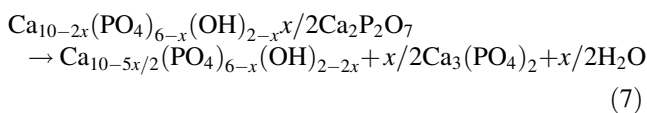


Table 2 shows the partial mass loss in this step. As we can see there is a significant difference in mass loss between samples containing high amount of DCPD (30c15m, 40c15m) instead of samples that not containing DCPD (60c120m, 50c120m).

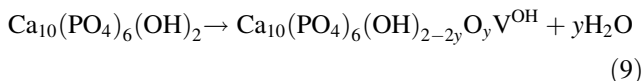
The transformations of acid-phosphate and DCPA ions to calcium pyrophosphate (CPP) take place in the third step at about 700–850 K during a second wide endothermic step (reactions 4, 5). In the same step the decomposition of OCP leads to the formation of CPP and  $\beta$ -TCP (reaction 5). The dramatical decrease of mass loss of this step ( $\sim 0.8\%$ ) for the 60c samples indicate the low CPP appearance in the previous step due to the absence of DCPD and DCPA phases.



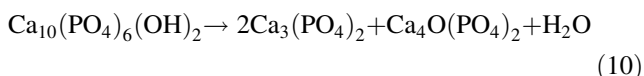
A wide peak in temperature range between 850 and 1,050 K is attributed to the reaction of HA with CPP leading to  $\beta$ -TCP production accordingly with reactions (7) and (8). In this step the average mass loss is up to ( $\sim 0.20\%$ ).



The partial dehydration (reaction 9) and HA decomposition (reaction 10) take place in the last step at temperature range between 1,050 and 1,300 K.



where  $\text{V}^{\text{OH}}$  denotes the OH lattice vacancies.



The average mass loss in this step is  $\sim 0.40\%$ .

## Conclusions

The calorimetric study of the calcium phosphate precipitation revealed the great influence of both time and temperature effect on the calcium phosphate precipitation.

Temperature seems to affect the solids' composition and textural properties in the final products while time leads this composition into the more stable form of HA. Normally a multi-phase system is obtained in the lower temperatures, which is slowly transformed into a biphasic system at higher temperatures and aging time. This project's results showed also the accordance of the XRD analysis to the TG/DTG/DSC proving that Thermal Analysis is a very useful tool on multiple phases systems' investigation.

## References

- Habraken WJEM, Wolke JGC, Jansen JA. Synthesis of nonporous calcium phosphate spheres using polyacrylic acid as structuring unit. *Adv Drug Deliv Rev.* 2007;59:234–48.
- Pang YX, Bao X. Influence of temperature, ripening time and calcinations on the morphology and crystallinity of hydroxyapatite nanoparticles. *J Eur Ceram Soc.* 2003;23:1697–704.
- Chaudhry AA, Haque S, Kellici S, Boldrin P, Rehman L, Khalid FA, et al. Instant nano-hydroxyapatite: a continuous and rapid hydrothermal synthesis. *Chem Commun.* 2006;21:286–8.
- Tas AC. Formation of calcium phosphate whiskers in hydrogen peroxide ( $\text{H}_2\text{O}_2$ ) solutions at 90 °C. *J Am Ceram Soc.* 2007;90:2358–62.
- Ma MG, Zhu YJ, Chang J. Solvothermal preparation of hydroxyapatite microtubes in water/N,N-dimethylformamide mixed solvents. *Mater Lett.* 2008;62:1642–5.
- He Q, Huang Z, Liu Y, Chen W, Xu T. Template-directed one-step synthesis of flowerlike porous carbonated hydroxyapatite spheres. *Mater Lett.* 2007;61:141–3.
- Oktar FN. Microstructure and mechanical properties of sintered enamel. *Hydroxyapatite. Ceram Intern.* 2007;33:1309–14.
- Markovic M, Fowler BO, Tung MS. Preparation and comprehensive characterization of a calcium hydroxyapatite. *J Res Natl Inst Stand Technol.* 2004;109(6):553–68.
- Wang Y, Zhang S, Wei K, Zhao N, Chen J, Wang XD. Hydrothermal synthesis of hydroxyapatite nanopowders using cationic surfactant as a template. *Mater Lett.* 2006;60:1484–7.
- Livingston TL, Gordon S, Archambault M, Kadiyala S, McIntosh K, Smith A, et al. Mesenchymal stem cells combined with biphasic calcium phosphate ceramics promote bone regeneration. *J Mater Sci: Mater Med.* 2003;14:211–8.
- Riman RE, Suchanek WL, Byrappa K, Chen CW, Shuk P, Oakes CS. Solution synthesis of hydroxyapatite designer particulates. *Solid State Ionics.* 2002;151:393–402.
- Mezahi FZ, Oudadesse H, Harabi A, Lucas-Girot A, Le Gal Y, Chaair H, et al. Dissolution kinetic and structural behavior of natural hydroxyapatite vs. thermal treatment. *J Therm Anal Calorim.* 2009;95:21–9.
- Bianco A, Cacciotti I, Lombardi M, Montanaro L, Gusmano G. Thermal stability and sintering behavior of hydroxyapatite nanopowders. *J Therm Anal Calorim.* 2007;88:237–43.
- Koumoulidis GC, Vaimakis TC, Sdoukos AT, Boukos NK, Trapalis SS. Preparation of hydroxyapatite lath-like using high-speed dispersing equipment. *J Am Ceram Soc.* 2001;84:1203–8.
- Koumoulidis GC, Trapalis CC, Vaimakis TC. Sintering of hydroxyapatite lath-like powders. *J Therm Anal Calorim.* 2006;84:165–74.